

Surface tension of compressed, superheavy atoms

Jorge A. Rueda, Yuan-Bin Wu[‡], and She-Sheng Xue

Dipartimento di Fisica and ICRA, Sapienza Università di Roma, Piazzale Aldo Moro 5,
I-00185 Rome, Italy
ICRANet, Piazza della Repubblica 10, I-65122 Pescara, Italy

Abstract. Based on the relativistic mean field theory and the Thomas-Fermi approximation, we study the surface properties of compressed, superheavy atoms. By compressed, superheavy atom we mean an atom composed by a superheavy nuclear core (superheavy nucleus) with mass number of the order of 10^4 , and degenerate electrons that neutralize the system. Some electrons penetrate into the superheavy nuclear core and the rest surround it up to a distance that depends upon the compression level. Taking into account the strong, weak, and electromagnetic interactions, we numerically study the structure of compressed, superheavy atoms and calculate the nuclear surface tension and Coulomb energy. We analyze the influence of the electron component and the background matter on the nuclear surface tension and Coulomb energy of compressed, superheavy atoms. We also compare and contrast these results in the case of compressed, superheavy atoms with phenomenological results in nuclear physics and the results of the core-crust interface of neutron stars with global charge neutrality. Based on the numerical results we study the instability against Bohr-Wheeler surface deformations in the case of compressed, superheavy atoms. The results in this article show the possibility of the existence of such compressed, superheavy atoms, and provide the evidence of strong effects of the electromagnetic interaction and electrons on the structure of compressed, superheavy atoms.

PACS numbers: 21.10.-k, 05.30.Fk, 26.60.-c

1. Introduction

It has been shown recently that the Einstein-Maxwell-Thomas-Fermi (EMTF) equations [1] supersede the traditional Tolman-Oppenheimer-Volkoff (TOV) [2, 3] equations used for the construction of neutron star equilibrium configurations, when taking into account the strong, weak, electromagnetic, and gravitational interactions. In contrast to the imposing of the condition of local charge neutrality in the traditional TOV approach, the condition of global charge neutrality is applied in the EMTF approach, owing to the fact that the traditional treatment imposing the condition of local charge neutrality is not consistent with the field equations and microphysical conditions of equilibrium for the system of neutrons, protons, and electrons in β equilibrium and obeying relativistic quantum statistics [4].

In order to describe the strong interactions between nucleons, the σ - ω - ρ nuclear model of relativistic mean field theory (RMFT) [5–12] is adopted in the EMTF approach. This model contains Dirac nucleons together with a scalar meson σ and a vector meson ω as well as an isovector meson ρ . The RMFT has gained great successes in giving a quantitative description of nuclear properties [13–15] and understanding the inhomogeneous structures of

[‡] send correspondence to wuyb@icranet.org

[§] Present address: Max-Planck-Institut für Kernphysik, Saupfercheckweg 1, D-69117 Heidelberg, Germany

low-density nuclear matter which can be realized in supernovae cores or in neutron star crusts (see e.g. Refs. [16–26] about the nuclear pasta structures).

As shown in Ref. [27], the self-consistent solution of the EMTF equations leads to a new structure of neutron stars, which is significantly different from the neutron star structure obtained from the TOV equations imposing local charge neutrality [28]. In this new structure of neutron stars, a transition layer (interface) appears between the core and the crust of the star, near the nuclear saturation density. There is a discontinuity in the density at the core-crust transition in this new structure of neutron stars. The core (bulk region) inside this transition layer is a hadronic phase and the crust outside this transition layer is composed of a nuclei lattice and relativistic degenerate electrons and possibly neutrons at densities below the nuclear saturation density and higher than the estimated neutron-drip value $\sim 4.3 \times 10^{11} \text{ g cm}^{-3}$ [29, 30]. Inside the transition region, a very strong electric field overwhelming the critical field $E_c = m_e^2 c^3 / (e\hbar)$ for vacuum breakdown appears [27], where m_e is the electron mass.

The surface properties of nuclear matter such as the surface tension and the curvature energy play an important role in many situations and phenomena such as the stability of nuclei, fragment distributions in heavy-ion collisions, and phase transitions between different phases of nuclear matter. The surface properties of nuclear matter have been analyzed a lot in the past few decays for the matter at the nuclear saturation density [9, 31–39], as well as the matter at the supranuclear regime realized in the interior of neutron stars [40, 41] for the phase transition region and the pasta structures of the low-density nuclear matter [16–18, 20].

The surface properties of the core-crust interface of the new neutron star structure obtained from the solution of the EMTF equations has been studied in Ref. [42] (see also Ref. [43] for a brief description). We calculated in Ref. [42] the surface tension as well as the electrostatic energy stored in this core-crust transition layer. We analyzed the stability of these systems through the Bohr-Wheeler fission mechanism [44]. It was shown in Ref. [42] that the electromagnetic interaction and the presence of degenerate electrons have evident effects on the surface properties of the core-crust interface. In the analyses of Refs. [27, 42], we employed the condition that the electron density is approximately equal to the proton density in the core bulk region. Here we consider a more general case that the electron density is smaller than the proton density in core bulk region. Actually, this is the case of compressed, superheavy atoms in which some of the electrons have penetrated into superheavy nuclear cores (superheavy nuclei) [45, 46] (we call them compressed, superheavy atoms according to Ref. [46] in which a similar object was studied). A compressed, superheavy atom is an atom composed by a superheavy nuclear core (superheavy nucleus), and degenerate electrons that neutralize the system. Some electrons penetrate into the superheavy nuclear core and the rest surround it up to a distance that depends upon the compression level. Such kind of compressed, superheavy atoms are hypothetical objects and could be possible to appear in the high density region of the neutron star crust or in other systems for example in the r-processes in gamma-ray bursts; studies of such kind of objects could provide a better understanding in the field of nuclear physics and nuclear astrophysics. In this article, we study the surface properties of these compressed, superheavy atoms.

The article is organized as follows. In Sec. 2, we formulate the relativistic equations of motion for the system of neutrons, protons and electrons fulfilling the strong and electromagnetic interactions and β equilibrium, and the equations for governing the nuclear surface tension and Coulomb energy of compressed, superheavy atoms. In Sec. 3, we present our discussions on the basis of the numerical analysis of the structure, the nuclear surface tension, and the Coulomb energy of compressed, superheavy atoms. We also apply the Bohr-Wheeler fission mechanism [44] to analyze the stability of compressed, superheavy atoms, in

Sec. 3. We finally give a summary in Sec. 4. We use units with $\hbar = c = 1$ throughout the article.

2. Equations of motion and surface tension

The system of compressed, superheavy atoms under consideration is composed of degenerate neutrons, protons, and electrons including the strong, electromagnetic, and weak interactions and fulfilling global charge neutrality. In this system, the electron density in the inside bulk region (n_{eb}) smaller than the proton one (n_{bp}), i.e., $n_{eb} < n_{bp}$. We adopt the σ - ω - ρ phenomenological nuclear model of Boguta and Bodmer [9] to describe the strong interactions between the nucleons. The Lagrangian density of the model we considered here is given by

$$\mathcal{L} = \mathcal{L}_f + \mathcal{L}_\sigma + \mathcal{L}_\omega + \mathcal{L}_\rho + \mathcal{L}_\gamma + \mathcal{L}_{int}, \quad (1)$$

including the free-field Lagrangian densities \mathcal{L}_γ , \mathcal{L}_σ , \mathcal{L}_ω , and \mathcal{L}_ρ , respectively for the electromagnetic and the three mesonic fields, the three fermion species (electrons, protons and neutrons) Lagrangian density \mathcal{L}_f and the interacting part \mathcal{L}_{int} . A detailed description of this model can be found in Ref. [27].

We adopt the compressed, superheavy atom as a spherical droplet, so we have spherical symmetry in this system. Within the mean-field approximation and Thomas-Fermi approximation, the equations of motion for this system are given by

$$\frac{d^2 V}{dr^2} + \frac{2}{r} \frac{dV}{dr} = -4\pi e(n_p - n_e), \quad (2)$$

$$\frac{d^2 \sigma}{dr^2} + \frac{2}{r} \frac{d\sigma}{dr} = [\partial_\sigma U(\sigma) + g_s n_s], \quad (3)$$

$$\frac{d^2 \omega}{dr^2} + \frac{2}{r} \frac{d\omega}{dr} = -(g_\omega J_0^\omega - m_\omega^2 \omega), \quad (4)$$

$$\frac{d^2 \rho}{dr^2} + \frac{2}{r} \frac{d\rho}{dr} = -(g_\rho J_0^\rho - m_\rho^2 \rho), \quad (5)$$

$$E_e^F = \mu_e - eV = \text{constant}, \quad (6)$$

$$E_p^F = \mu_p + g_\omega \omega + g_\rho \rho + eV = \text{constant}, \quad (7)$$

$$E_n^F = \mu_n + g_\omega \omega - g_\rho \rho = \text{constant}. \quad (8)$$

This is a special case of the EMTF system of equations [1, 27] without the presence of the gravitational interaction. Here we have introduced the notation $\omega_0 \equiv \omega$, $\rho_0 \equiv \rho$, and $A_0 \equiv V$ for the time components of the meson fields, where A is the electromagnetic field.

$\mu_i = \sqrt{(P_i^F)^2 + \tilde{m}_i^2}$ and $n_i = (P_i^F)^3 / (3\pi^2)$ are the free chemical potential and the number density of the i -fermion species ($i = n, p, e$) with Fermi momentum P_i^F . The particle effective masses are $\tilde{m}_N = m_N + g_s \sigma$ and $\tilde{m}_e = m_e$, where m_i is the rest mass of each i -fermion species. g_s , g_ω , and g_ρ are the coupling constants of the σ , ω and ρ fields, and e is the fundamental electric charge. m_σ , m_ω , and m_ρ are the masses of σ , ω , and ρ . $U(\sigma)$ is the scalar self-interaction potential which can be found in e.g. Refs. [27, 42].

The generalized Fermi energies of electrons, protons, and neutrons, E_e^F , E_p^F , and E_n^F , derived from the thermodynamic equilibrium conditions given by the statistical physics of multicomponent systems, are linked by the β -equilibrium [47] of protons, neutrons, and electrons,

$$E_n^F = E_p^F + E_e^F. \quad (9)$$

The scalar density n_s is given by the expectation value

$$n_s = \frac{2}{(2\pi)^3} \sum_{i=n,p} \int_0^{P_i^F} d^3k \frac{\tilde{m}_N}{\varepsilon_i^k(k)}, \quad (10)$$

where $\varepsilon_i^k(k) = \sqrt{k^2 + \tilde{m}_i^2}$ is the single particle energy. In the static case, the nonvanishing components of the currents are

$$J_0^{ch} = (n_p - n_e), \quad (11)$$

$$J_0^{\omega} = n_b = (n_n + n_p), \quad (12)$$

$$J_0^{\rho} = (n_p - n_n), \quad (13)$$

here $n_b = n_p + n_n$ is the baryon number density.

We would like to mention here that the Thomas-Fermi approximation and the Thomas-Fermi approximation combined with the RMFT applied to nuclei are well-known and have gained great successes in understanding nuclear structures (see, e.g., Refs. [48–50]). In the present study, we apply this approach of the Thomas-Fermi approximation combined with RMFT to compressed, superheavy atoms, inspired by our new neutron star model studied in Refs. [27, 42]. One of our major purposes here is to analyze the possibility of the existence of such “exotic” neutron rich nuclei whose mass numbers are much larger than that of ordinary nuclei. Another major purpose here is to study the effects of the electrons and electromagnetic interaction on the surface properties of such a system. The study presented in this article would give us a further understanding of the influence of the electromagnetic interaction and electrons on the surface properties of the core-crust interface of our new structure of neutron stars [27, 42], hence give us a further understanding of global charge neutrality and the structure of neutron stars.

The parameters of the nuclear model, namely the coupling constants g_s , g_ω , and g_ρ , the meson masses m_σ , m_ω , and m_ρ , and the third- and fourth- order constants of the self-scalar interactions g_2 and g_3 are fixed by fitting nuclear experimental data, such as saturation density, binding energy per nucleon, symmetry energy, surface energy, and nuclear incompressibility. We here use the parameters of the NL3 parametrization [51] as the one used in Refs [27, 42], shown in Table 1.

m_σ (MeV)	508.194	g_ω	12.868
m_ω (MeV)	782.501	g_ρ	4.474
m_ρ (MeV)	763.000	g_2 (fm ⁻¹)	-10.431
g_s	10.217	g_3	-28.885

Table 1. The parameters of the nuclear model from NL3 [51].

Now we turn to the analyze of the surface tension of this system. We construct the surface tension following a similar method in Ref. [42]. Since we treat the compressed, superheavy atom as a spherical droplet, we assume a spherical surface (the size of the system under consideration is larger than the one of ordinary nuclei, so the nuclear curvature energy here is small compared to the nuclear surface energy) with a small thickness separating one finite region (inside the nuclear core region) and one semi-infinite region (outside background region, similar to the outside crust region in the discussion of Ref. [42]). The number density of the i -fermion species $n_i(r)$ approaches the density of the i -fermion species n_{ib} in the origin

(the inside region) as the position $r \rightarrow 0$, and approaches the density in the outside region of the i -fermion species n_{io} as the $r \rightarrow +\infty$. To construct the surface tension, as in the case of the semi-infinite matter model, we imagine a reference system with sharp surfaces at radii r_i ($i = n, p, e, \sigma, \omega, \rho$) at which fermion densities and meson fields fall discontinuously from the bulk region to the outside region. Following a similar method of Baym-Bethe-Pethick (BBP) [29], the location of the reference surface for the i -fermion species is defined by the condition that the reference system has the same number of i -fermion species as the original system,

$$4\pi \int_0^{r_i} r^2 dr [n_i(r) - n_{ib}] + 4\pi \int_{r_i}^{\infty} r^2 dr [n_i(r) - n_{io}] = 0, \quad i = n, p, e. \quad (14)$$

Similar to the definition of reference surfaces for fermions, the location of the reference surfaces for meson fields are defined by

$$4\pi \int_0^{r_i} r^2 dr [F_i(r) - F_{ib}] + 4\pi \int_{r_i}^{\infty} r^2 dr [F_i(r) - F_{io}] = 0, \quad i = \sigma, \omega, \rho, \quad (15)$$

where $F_i(r)$ is the time component of the i -meson field, F_{ib} is the time component of the i -meson field in the inside region, and F_{io} is the time component of the i -meson field in the outside region.

Similar to the way of BBP [29], the nuclear surface energy can be computed as the total energy subtracting off the bulk energy,

$$E_{\text{sur}} = \sum_{i=n,p,\sigma,\omega,\rho} 4\pi \left\{ \int_0^{r_i} r^2 [\varepsilon_i(r) - \varepsilon_{ib}] dr + \int_{r_i}^{\infty} r^2 [\varepsilon_i(r) - \varepsilon_{io}] dr \right\}, \quad (16)$$

and the Coulomb energy is

$$E_{\text{coul}} = 4\pi \int_0^{\infty} r^2 \varepsilon_E(r) dr, \quad (17)$$

where $\varepsilon_i(r)$ is the energy density of the i species of fermion or meson fields, ε_{ib} is the energy density of the i species of fermion or meson fields in the center of the system (the inside region), ε_{io} is the energy density of the i species of fermion or meson field in the outside region, and $\varepsilon_E(r)$ is the energy density of the electric field. Similar to the energy densities given in Ref. [42], the energy density of the i -fermion species $\varepsilon_i(r)$ is

$$\varepsilon_i(r) = \frac{1}{8\pi^2} \left\{ P_i^F \sqrt{(P_i^F)^2 + \tilde{m}_i^2} [2(P_i^F)^2 + \tilde{m}_i^2] - \tilde{m}_i^4 \ln \frac{P_i^F + \sqrt{(P_i^F)^2 + \tilde{m}_i^2}}{\tilde{m}_i} \right\}, \quad (18)$$

and the energy densities of the meson fields in this spherical system are

$$\varepsilon_{\sigma}(r) = \frac{1}{2} \left(\frac{d\sigma}{dr} \right)^2 + U(\sigma), \quad (19)$$

$$\varepsilon_{\omega}(r) = \frac{1}{2} \left(\frac{d\omega}{dr} \right)^2 + \frac{1}{2} m_{\omega}^2 \omega^2, \quad (20)$$

$$\varepsilon_{\rho}(r) = \frac{1}{2} \left(\frac{d\rho}{dr} \right)^2 + \frac{1}{2} m_{\rho}^2 \rho^2, \quad (21)$$

$$\varepsilon_E(r) = \frac{1}{8\pi} \left(\frac{dV}{dr} \right)^2. \quad (22)$$

The nuclear surface tension is given as the nuclear surface energy per unit area,

$$\sigma_{\text{Ns}} = \frac{E_{\text{sur}}}{4\pi r_n^2}, \quad (23)$$

and similarly we obtain the Coulomb energy per unit area (the surface tension for the electric field)

$$\sigma_{\text{Cs}} = \frac{E_{\text{coul}}}{4\pi r_n^2}, \quad (24)$$

where r_n is the reference radius of neutrons defined by Eq. (14). Since the neutron number is much larger than the proton number in the system, so it is reasonable to set the radius of neutrons to be the radius of the nucleus to estimate the surface tensions; this is consistent with the existence of the neutrons halo or neutron skin effect [52].

The relation between the nuclear surface energy and the Coulomb energy is very important for a nucleus. As shown by Bohr and Wheeler [44] when the condition

$$E_{\text{coul}} > 2E_{\text{sur}} \quad (25)$$

is satisfied, the nucleus becomes unstable against nuclear fission. A careful analysis on the derivation of this condition shows that the Bohr-Wheeler condition given by Eq. (25) applies also to our system [42].

3. Numerical analysis

Following a similar procedure in Refs. [27, 42], we can solve the equations (2)-(8) together with the β -equilibrium (9) to obtain the fermion-density and meson-field profiles. This system of equations can be numerically solved with appropriate boundary conditions and approximations, as shown in Refs. [27, 42].

In order to obtain a solution of these equations, we set a value for the baryon number density $n_{\text{bb}} = n_{nb} + n_{pb}$ in the region near the center, and we set a small electron density $n_{eb} = y_e n_{pb}$ in the region near the center with electron fraction $y_e < 1$. As described in Refs. [27, 42], the fermion densities n_{io} in the outside region depend on the density at the base of the background under consideration (similar to the crust in the discussion of Ref. [42]). The background matter is composed of a nuclei lattice in a background of degenerate electrons, whose density is denoted here as n_e^{bg} . In addition, there are free neutrons in the background when the density ρ_{bg} of the background is higher than the neutron-drip density $\rho_{\text{drip}} \approx 4.3 \times 10^{11} \text{ g cm}^{-3}$ [29]. So when the density ρ_{bg} of the background is smaller than the neutron-drip density ρ_{drip} , i.e., $\rho_{\text{bg}} < \rho_{\text{drip}}$, we set the proton density and the neutron density to zero in the outside region while the electron density matches the value n_e^{bg} of the density of background electrons, i.e., $n_{eo} = n_e^{\text{bg}}$. When $\rho_{\text{bg}} > \rho_{\text{drip}}$ both the neutron density and the electron density have to match their corresponding background densities, i.e., $n_{eo} = n_e^{\text{bg}}$ and $n_{no} = n_n^{\text{bg}}$, where n_n^{bg} is the neutron density in the background. As shown in Ref. [29] there is no proton drip in the systems under consideration, so we keep the outside proton density value as zero. In order to set the matching density values for electrons and neutrons we use the relation between the free neutron density and the electron density in Section 6 of Ref. [29].

As shown in Refs. [27, 42], the transition interface that we are interesting in appears near the nuclear saturation density $n_{\text{nucl}} = 0.16 \text{ fm}^{-3}$. In order to study the compressed, superheavy atoms and the influence of the electrons and electromagnetic interaction on the surface properties of the system, we assume at first the baryon number density in the region near the center to be the nuclear saturation density (results presented in Figs. 1-5), i.e.,

$n_{\text{bb}} = n_{\text{nucl}} = 0.16 \text{ fm}^{-3}$. At the end of this section, we will also study the influence of baryon number density (results presented in Fig. 6 and Table 2).

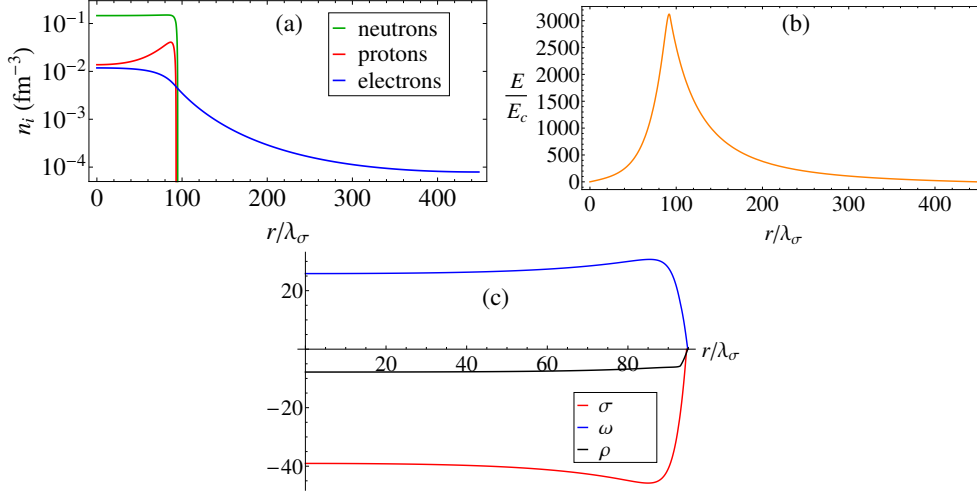


Figure 1. (Color online) (a): fermion density profiles in units of fm^{-3} . (b): electric field in units of the critical field E_c . (c): meson fields σ , ω , and ρ in units of MeV. Here we set $P_{\text{eb}}^F = 0.95 P_{\text{pb}}^F$, the baryon number density in the region near the center is the nuclear saturation density n_{nucl} , and the density in the outside (background) region is the neutron-drip density $\rho_{\text{bg}} = \rho_{\text{drip}} \approx 4.3 \times 10^{11} \text{ g cm}^{-3}$. $\lambda_\sigma = \hbar/(m_\sigma c) \sim 0.4 \text{ fm}$ is the Compton wavelength of the σ meson.

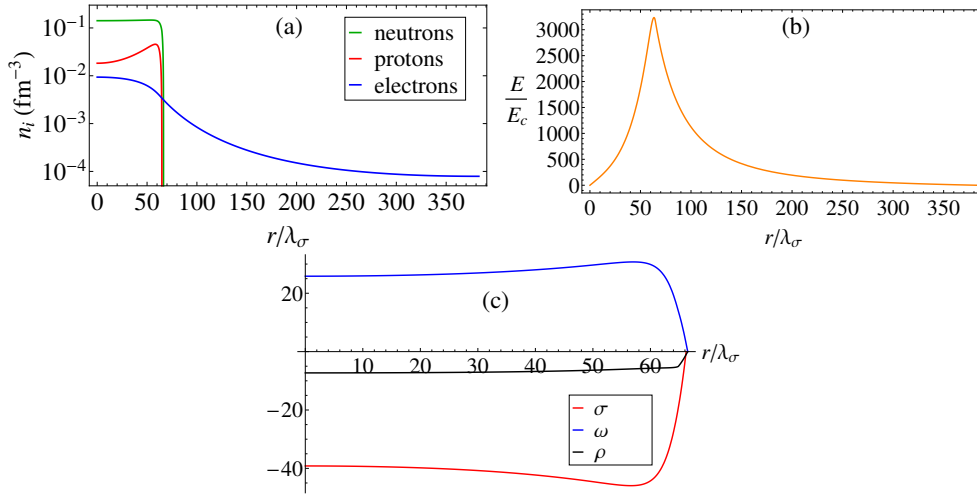


Figure 2. (Color online) (a): fermion density profiles in units of fm^{-3} . (b): electric field in units of the critical field E_c . (c): meson fields σ , ω , and ρ in units of MeV. Here we set $P_{\text{eb}}^F = 0.8 P_{\text{pb}}^F$, the baryon number density in the region near the center is the nuclear saturation density n_{nucl} , and the density in the outside (background) region is the neutron-drip density $\rho_{\text{bg}} = \rho_{\text{drip}} \approx 4.3 \times 10^{11} \text{ g cm}^{-3}$.

The results of the solutions of two examples are shown in Fig. 1 for the case $P_{\text{eb}}^F = 0.95P_{\text{pb}}^F$ and in Fig. 2 for the case $P_{\text{eb}}^F = 0.8P_{\text{pb}}^F$, when the density in the outside (background) region is the neutron-drip density $\rho_{\text{bg}} = \rho_{\text{drip}} \approx 4.3 \times 10^{11} \text{ g cm}^{-3}$. We have introduced the notations P_{eb}^F for the Fermi momentum of electrons in the region near the center of the system, and P_{pb}^F for the Fermi momentum of protons in the region near the center of the system. It is also worth mentioning here that the typical mass number of these compressed, superheavy atoms is $\sim 10^4$; e.g., $A \sim 35000$ and $Z/A \sim 0.154$ for the case shown in Fig. 1, and $A \sim 12000$ and $Z/A \sim 0.189$ for the case shown in Fig. 2, where A is the total number of nucleons (mass number) and Z is the total number of protons. The mass numbers of these compressed, superheavy atoms are much larger than that of ordinary nuclei.

As shown in Fig. 1, when the difference between the electron density and the proton density in the region near the center of the system ($n_{\text{pb}} - n_{\text{eb}}$) is small, the fermion-density and meson-field profiles are similar to their counterparts in the case of semi-infinite matter (electron density nearly equal to the proton density in the inside bulk region $n_{\text{eb}} \simeq n_{\text{pb}}$). Comparing to the results in the case of the electron density being approximately equal to the proton density in the core bulk region shown in Ref. [42], the bump of the proton profile is larger in this case, as expected from the fact that the internal electric field is less screened than the case of $n_{\text{eb}} \simeq n_{\text{pb}}$. We can also see from Figs. 1-2, how the fermion and meson-field profiles change for increasing charge separations ($n_{\text{pb}} - n_{\text{eb}}$).

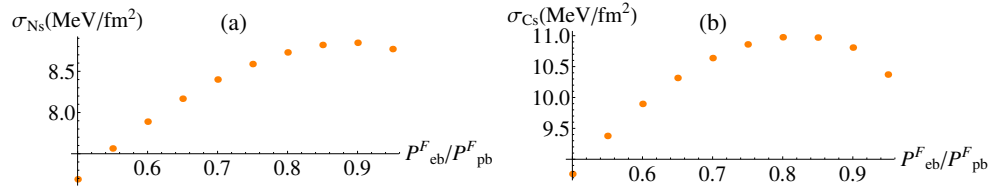


Figure 3. (Color online) The dependence of the surface tension on the ratio $P_{\text{eb}}^F/P_{\text{pb}}^F$. The baryon number density in the region near the center is the nuclear saturation density n_{nucl} , and the fermion densities and meson fields tend to be zero in the outside region. (a): nuclear surface tension σ_{N_s} . (b): Coulomb energy per unit area σ_{C_s} .

Using the definitions in Eqs. (23) and (24), we obtain the surface tensions for compressed, superheavy atoms. The dependence of the surface tension on the ratio of the electron Fermi momentum and the proton Fermi momentum in the region near the center of the system ($P_{\text{eb}}^F/P_{\text{pb}}^F$) is shown in Fig. 3 for the case of the fermion densities and meson fields tending to be zero in the outside region, and Fig. 4 for the case of the density in the outside (background) region is the neutron-drip density $\rho_{\text{bg}} = \rho_{\text{drip}} \approx 4.3 \times 10^{11} \text{ g cm}^{-3}$. From the results, the system is stable with respect to the Bohr-Wheeler condition (25) of the stability, in all ratios $P_{\text{eb}}^F/P_{\text{pb}}^F$ we consider. This is the result of the penetration of the relativistic electrons into the nucleus (see also Refs. [45, 46]). This in principle implies the possibility of the existence of such kind of compressed, superheavy atoms. As shown in Fig. 3, the nuclear surface tension σ_{N_s} first increases and then decreases when the difference between the electron density and the proton density increases, and the nuclear surface tension tends to the phenomenological result ($\sim 1 \text{ MeV fm}^{-2}$) without the presence of electrons in the inside bulk region studied in the nuclear physics [29]. There are two effects which influence on the nuclear surface tension σ_{N_s} : (I) for $n_{\text{eb}} < n_{\text{pb}}$ the bump of the proton profile around the nuclear surface changes as shown in Figs. 1–2, and (II) the higher the difference ($n_{\text{pb}} - n_{\text{eb}}$) is, the lower the nuclear asymmetry. As a consequence, the total energy of the system decreases.

The combination of these two effects leads to the results of the nuclear surface tension σ_{Ns} shown in Fig. 3.

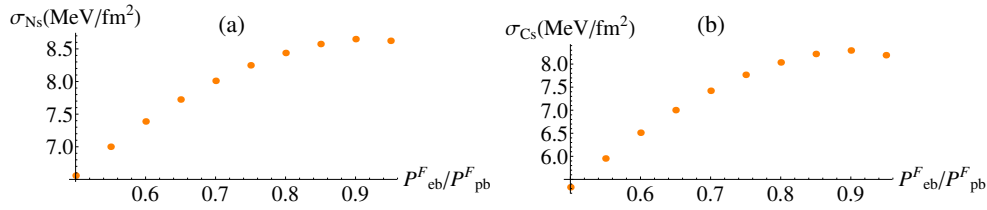


Figure 4. (Color online) The dependence of the surface tension on the ratio P_{eb}^F/P_{pb}^F . The baryon number density in the region near the center is the nuclear saturation density n_{nucl} , and the density in the outside region is the neutron-drip density $\rho_{\text{bg}} = \rho_{\text{drip}} \approx 4.3 \times 10^{11} \text{ g cm}^{-3}$. (a): nuclear surface tension σ_{Ns} . (b): Coulomb energy per unit area σ_{Cs} .

Comparing the results of Fig. 3 and Fig. 4, we can find that the electrons in the outside region have strong effects on the surface structure of compressed, superheavy atoms considered here. The increase of the electron density in the outside region effectively reduces the Coulomb energy per unit area σ_{Cs} , as well as the nuclear surface tension σ_{Ns} . This effect is enhanced when increasing difference between the electron density and the proton density in the region near the center of the system ($n_{pb} - n_{eb}$), as shown in Figs. 3-4. This effect is mainly due to the reason that the electrons have a strong influence on the bump on the profiles, leading to a strong effect on the surface structure and the surface tensions σ_{Ns} and σ_{Cs} . These results provide the evidence of strong effects of the electromagnetic interaction and electrons on structure of the system. This result of the effect due to the electrons in the outside region as shown by the comparison of Fig. 3 and Fig. 4 is different from the case studied in Ref. [42] where the electron density in the inside bulk region (n_{eb}) is nearly equal to the proton one (n_{bp}). In the case shown in Ref. [42], the effect of the electrons in the outside region is small when the density ρ_{bg} in the outside region is smaller than the neutron-drip density, $\rho_{\text{bg}} < \rho_{\text{drip}}$.

We now turn to study the effect of the free neutrons in the background (the outside region) on the surface properties of compressed, superheavy atoms. The dependence of the surface tension on the density ρ_{bg} of the background for the case of $P_{eb}^F = 0.8P_{pb}^F$ is shown in Fig. 5. As shown in Fig. 5(c), the Bohr-Wheeler condition (25) for the instability is reached at a background density $\rho_{\text{bg}}^{\text{crit}} \sim 9.7 \times 10^{13} \text{ g cm}^{-3}$, so the system becomes unstable against fission when $\rho_{\text{bg}} > \rho_{\text{bg}}^{\text{crit}}$. This imposes a physical upper limit to the density of the background for compressed, superheavy atoms with $P_{eb}^F = 0.8P_{pb}^F$. This critical background density $\rho_{\text{bg}}^{\text{crit}}$ is smaller than the one for the case of the electron density in the inside bulk region being nearly equal to the proton one ($n_{eb} \simeq n_{bp}$) discussed in Ref. [42]. This implies that the difference between the electron density and the proton density in the region near the center of the system ($n_{pb} - n_{eb}$) can decrease the stability of compressed, superheavy atoms.

The results in Fig. 5 clearly show the strong effect of the fermions in the outside (background) region on the surface structure of compressed, superheavy atoms, as we have discussed above in the comparison of Fig. 3 and Fig. 4. The Coulomb energy per unit area σ_{Cs} and the nuclear surface tension σ_{Ns} change significantly as changing the density ρ_{bg} of the background (the outside region), in both cases: (I) the density ρ_{bg} of the background is higher than the neutron-drip density ρ_{drip} ; (II) the density ρ_{bg} of the background is smaller than the neutron-drip density ρ_{drip} .

In the previous discussions, we have assumed the baryon number density in the region

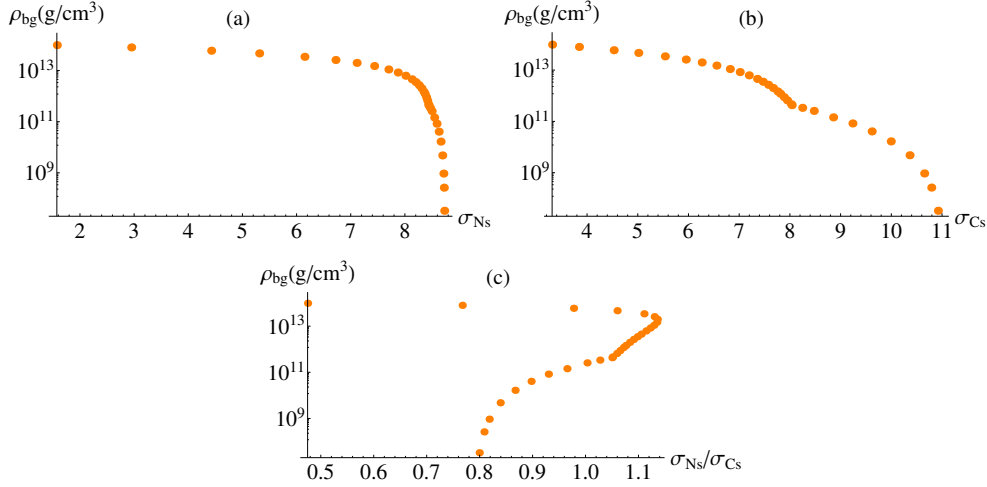


Figure 5. (Color online) The dependence of the surface tension on the density ρ_{bg} of the background. Here we set $P_{eb}^F = 0.8P_{pb}^F$ and the baryon number density in the region near the center is the nuclear saturation density n_{nucl} . (a): nuclear surface tension σ_{Ns} , in units of MeV fm^{-2} . (b): Coulomb energy per unit area σ_{Cs} , in units of MeV fm^{-2} . (c) Ratio of the nuclear surface tension and the Coulomb energy per unit area, σ_{Ns}/σ_{Cs} .

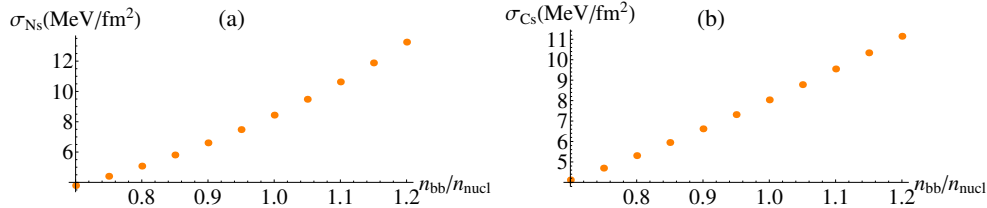


Figure 6. (Color online) The dependence of the surface tension on the baryon number density in the region near the center (n_{bb}). Here $P_{eb}^F = 0.8P_{pb}^F$, and the density in the outside region is the neutron-drip density $\rho_{bg} = \rho_{drip} \approx 4.3 \times 10^{11}$ g cm^{-3} . (a): nuclear surface tension σ_{Ns} . (b): Coulomb energy per unit area σ_{Cs} .

near the center to be the nuclear saturation density n_{nucl} in symmetric matter, to study the influence of the electrons on the surface properties of the transition interface [27, 42]. However, the saturation density in nuclei can be different while changing the asymmetry parameter (see, e.g., Refs. [53, 54]). Therefore, it would be necessary to analyze the influence of the baryon number density on the surface tensions. The dependence of the surface tension on the baryon number density in the region near the center (n_{bb}) is shown in Fig. 6, for the case of $P_{eb}^F = 0.8P_{pb}^F$ and $\rho_{bg} = \rho_{drip} \approx 4.3 \times 10^{11}$ g cm^{-3} . Comparing with the results in Ref. [42], the dependence of the surface tension on the baryon number density shown in Fig. 6 for the case of compressed, superheavy atoms has a similar behavior as in the case discussed in Ref. [42] for the core-crust interface of neutron stars ($n_{eb} \approx n_{pb}$). Therefore, we can conclude that the effects of the baryon number density on the surface tensions σ_{Ns} and σ_{Cs} for the case of compressed, superheavy atoms are similar to the ones for the case the core-crust interface of neutron stars ($n_{eb} \approx n_{pb}$) [42].

$P_{\text{eb}}^F/P_{\text{pb}}^F$	σ_{Ns}	σ_{Cs}	$E_{\text{sur}}/A^{2/3}$
0.5	3.84	3.57	69.7
0.8	5.07	5.31	90.4
0.95	5.17	5.36	93.1

Table 2. Surface tensions σ_{Ns} and σ_{Cs} in MeV fm^{-2} and nuclear surface energy per surface nucleon $E_{\text{sur}}/A^{2/3}$ in MeV for selected values of $P_{\text{eb}}^F/P_{\text{pb}}^F$. Here the density in the outside region is the neutron-drip density $\rho_{\text{bg}} = \rho_{\text{drip}} \approx 4.3 \times 10^{11} \text{ g cm}^{-3}$, and the baryon number density in the region near the center (n_{bb}) is equal to $0.8n_{\text{nucl}}$.

Furthermore, we show in Table 2 the surface tensions of compressed, superheavy atoms for selected values of $P_{\text{eb}}^F/P_{\text{pb}}^F$ when a smaller baryon number density in the region near the center is adopted ($n_{\text{bb}} = 0.8n_{\text{nucl}}$). We can learn from Table 2 and Fig. 4 that the dependence of the surface tension on the ratio $P_{\text{eb}}^F/P_{\text{pb}}^F$ for the case of compressed, superheavy atoms with a smaller baryon number density in the region near the center has a similar behavior as in the case when the baryon number density in the region near the center is n_{nucl} .

It is worth mentioning that the properties of medium-mass and heavy nuclear clusters embedded in a gas of nucleons were analyzed in Refs. [53, 54]. The calculations varying the cluster size and isospin asymmetry over a large domain of N (neutron number) and Z covering the whole periodic table well beyond the neutron drip line, were performed. The nuclear surface energy per surface nucleon $E_{\text{sur}}/A^{2/3}$ obtained in Refs. [53, 54] is in the order of 20 MeV (the value depends on the parameters such as the asymmetry of the nucleus and the density of the nucleon gas [53, 54]). Comparing the result shown in Table 2 and the result obtained in Refs. [53, 54], compressed, superheavy atoms under consideration have larger nuclear surface energies per surface nucleon $E_{\text{sur}}/A^{2/3}$. This is mainly due to the fact that the electromagnetic interaction and the presence of electrons change the proton and neutron density profiles, as we have discussed in Ref. [42]. As we have shown in Ref. [42], the nuclear surface tension we obtained for the case without the presence of electrons matches the result in literature for ordinary nuclear matter. The trend from compressed, superheavy atoms to ordinary nuclei is also shown in Figs. 3-4 and Table 2 when reducing the electron density.

4. Summary

Following our study [42] of the surface properties of the core-crust interface of neutron stars with global charge neutrality, we study the surface properties of compressed, superheavy atoms. By compressed, superheavy atom we mean an atom composed by a superheavy nuclear core (superheavy nucleus) with mass number of the order of 10^4 , and degenerate electrons that neutralize the system. Some electrons penetrate into the superheavy nuclear core and the rest surround it up to a distance that depends upon the compression level. We have adopted both the Thomas-Fermi approximation and RMFT approach and taken into account the strong, weak, and electromagnetic interactions. We numerically studied the structure of compressed, superheavy atoms, computed the nuclear surface tension and Coulomb energy of compressed, superheavy atoms, and analyzed the influence of the electron component and the background matter on the properties of these compressed, superheavy atoms.

We assume at first the baryon number density in the region near the center to be the nuclear saturation density n_{nucl} as in Ref. [42]. We show how the nuclear surface tension

σ_{N_s} and the Coulomb energy per unit area σ_{C_s} are drastically affected by the decreasing of electron to proton density ratio in the region near the center of compressed, superheavy atoms (see Figs. 1, 2, 3, and 4). This is due to the increasing of proton repulsion and the decreasing of nuclear asymmetry when decreasing electron to proton density ratio in the region near the center of compressed, superheavy atoms. If the charge separation is small (i.e., the electron density n_{eb} in the inside region is slightly smaller than the proton one n_{pb} ; it means most of electrons penetrate into nuclear cores), the surface properties are closed to the ones discussed in Ref. [42] for the core-crust interface of neutron stars ($n_{eb} \approx n_{pb}$). If the charge separation is large (i.e., the electron density in the inside region is much smaller than the proton one n_{pb} ; it means only some of electrons penetrate into nuclear cores), the surface properties approach to the results without the presence of electrons inside nuclei, studied in the nuclear physics.

It is also shown (see Figs. 3, 4, and 5) that electrons in the outside (background) region have strong effects on the surface properties of compressed, superheavy atoms. The increase of the electron density in the outside region effectively reduces the Coulomb energy per unit area σ_{C_s} and nuclear the surface tension σ_{N_s} even if the density ρ_{bg} of the background (the outside region) is smaller than the neutron-drip density ρ_{drip} . This effect is enhanced when increasing difference between the electron density and the proton density in the region near the center of the system ($n_{pb} - n_{eb}$) (the inside region). These results show the evidence of strong effects of the electromagnetic interaction and electrons on the structure of compressed, superheavy atoms.

Base on the above numerical results, we studied the instability of compressed, superheavy atoms against Bohr-Wheeler surface deformations. We find that the instability sets in at a critical density of the background $\rho_{bg}^{crit} \sim 9.7 \times 10^{13} \text{ g cm}^{-3}$ for compressed, superheavy atoms with $P_{eb}^F = 0.8P_{pb}^F$. This critical background density ρ_{bg}^{crit} is smaller than the one obtained in Ref. [42], where the electron density in the inside bulk region is nearly equal to the proton one ($n_{eb} \simeq n_{pb}$). This implies that the stability of the system can be decreased by increasing difference between the electron density and the proton density in the region near the center of compressed, superheavy atoms ($n_{pb} - n_{eb}$).

We also studied the influence of the baryon number density on the nuclear surface tension and the Coulomb energy per unit area of compressed, superheavy atoms. The results show that the effects of the baryon number density on the surface tensions σ_{N_s} and σ_{C_s} for the case of compressed, superheavy atoms are similar to the ones for the case the core-crust interface of neutron stars ($n_{eb} \approx n_{pb}$) [42].

We showed through the Bohr-Wheeler condition, the possibility of the existence of compressed, superheavy atoms with A in the order of 10^4 . The mass number of such kind of ‘‘exotic’’ neutron rich nuclei is about one order of magnitude larger than the usual neutron rich nuclei of the mass number being usually up to the order of 10^3 , studied in various models such as pasta structures (see, e.g., Refs. [20–24]) and heavy nuclear clusters (see, e.g., Refs. [53, 54]). Such kind of compressed, superheavy atoms could be possible to appear in the high density region of the neutron star crust or in the r-processes in gamma-ray bursts, since their existence is possible according to the Bohr-Wheeler condition as discussed in the present paper.

The results of this work show the effects of the electrons and electromagnetic interaction on the surface properties of the system composed of degenerate neutrons, protons, and electrons fulfilling global charge neutrality. This would give us a further understanding of the core-crust interface of our new structure of neutron stars analyzed in Refs. [27, 42].

To end this article, we would like to mention that another kind of instability in nuclear matter, corresponding to the transition density from nonuniform to uniform nuclear matter,

are widely discussed in the literature (see, e.g., Refs. [17, 18, 20, 26, 55, 56]). When the density reaches this transition density, the pasta structures become unstable and are dissolved into uniform matter. The transition density from nonuniform to uniform nuclear matter is around $\sim 0.08 \text{ fm}^{-3}$, and strongly depends on approach to obtain it; it can vary from $\sim 0.1 \text{ fm}^{-3}$ to $\sim 0.05 \text{ fm}^{-3}$ in different parameters of nuclear model (see, e.g., Refs. [17, 18, 20, 26, 55, 56]). This transition density from nonuniform to uniform nuclear matter is in the same order of the instability (critical) density obtained in the present article (baryon number density $\sim 0.05 \text{ fm}^{-3}$ for the case of $P_{\text{eb}}^F = 0.8P_{\text{pb}}^F$) and in Ref. [42] (baryon number density $\sim 0.07 \text{ fm}^{-3}$ for the case of $n_{\text{eb}} \simeq n_{\text{bp}}$ presented in Ref. [42]). It would be interesting to compare and contrast the instability mechanism analyzed in the present article and in Ref. [42] with the one of the transition density from nonuniform to uniform nuclear matter in the literature, and analyze the difference and links between these two instability mechanisms. However, these studies are out of the scope of this work and we leave these studies for future work.

Acknowledgments

Yuan-Bin Wu acknowledges the support given by the Erasmus Mundus Joint Doctorate Program under the Grant Number 2011-1640 from the EACEA of the European Commission, during which part of this work was developed.

- [1] J. A. Rueda, R. Ruffini, and S.-S. Xue, Nucl. Phys. A 872, 286 (2011).
- [2] R. C. Tolman, Phys. Rev. 55, 364 (1939).
- [3] J. R. Oppenheimer and G. Volkoff, Phys. Rev. 55, 374 (1939).
- [4] M. Rotondo, J. A. Rueda, R. Ruffini, and S.-S. Xue, Phys. Lett. B 701, 667 (2011).
- [5] H. P. Duerr, Phys. Rev. 103, 469 (1956).
- [6] L. D. Miller and A. E. S. Green, Phys. Rev. C 5, 241 (1972).
- [7] J. D. Walecka, Ann. Phys. 83, 491 (1974).
- [8] J. Boguta and J. Rafelski, Phys. Lett. B 71, 22 (1977).
- [9] J. Boguta and A. R. Bodmer, Nucl. Phys. A 292, 413 (1977).
- [10] J. Boguta and H. Stocker, Phys. Lett. B 120, 289 (1983).
- [11] J. Boguta and S. A. Moszkowski, Nucl. Phys. A 403, 445 (1983).
- [12] J. Boguta, Nucl. Phys. A 501, 637 (1989).
- [13] B. D. Serot, Rept. Prog. Phys. 55, 1855 (1992).
- [14] P. Ring, Prog. Part. Nucl. Phys. 37, 193 (1996).
- [15] M. Bender, P.-H. Heenen, and P.-G. Reinhard, Rev. Mod. Phys. 75, 121 (2003).
- [16] T. Maruyama, T. Tatsumi, D. N. Voskresensky, T. Tanigawa, and S. Chiba, Phys. Rev. C 72, 015802 (2005).
- [17] K. Oyamatsu and K. Iida, Phys. Rev. C 75, 015801 (2007).
- [18] S. S. Avancini, D. P. Menezes, M. D. Alloy, J. R. Marinelli, M. M. W. Moraes, and C. Providência, Phys. Rev. C 78, 015802 (2008).
- [19] M. Okamoto, T. Maruyama, K. Yabana, and T. Tatsumi, Phys. Lett. B 713, 284 (2012).
- [20] F. Grill, C. Providência, and S. S. Avancini, Phys. Rev. C 85, 055808 (2012).
- [21] S. S. Bao and H. Shen, Phys. Rev. C 89, 045807 (2014).
- [22] S. S. Bao and H. Shen, Phys. Rev. C 91, 015807 (2015).
- [23] W. G. Newton and J. R. Stone, Phys. Rev. C 79, 055801 (2009).
- [24] B. Schuetrumpf and W. Nazarewicz, Phys. Rev. C 92, 045806 (2015).
- [25] I. Sagert, G. I. Fann, F. J. Fattoyev, S. Postnikov, and C. J. Horowitz, Phys. Rev. C 93, 055801 (2016).
- [26] H. Pais and C. Providência, Phys. Rev. C 94, 015808 (2016).
- [27] R. Belvedere, D. Pugliese, J. A. Rueda, R. Ruffini, and S.-S. Xue, Nucl. Phys. A 883, 1 (2012).
- [28] P. Haensel, A. Y. Potekhin, and D. G. Yakovlev, Neutron Stars 1: Equation of State and Structure, Springer-Verlag, New York, 2007.
- [29] G. Baym, H. A. Bethe, and C. J. Pethick, Nucl. Phys. A 175, 225 (1971).
- [30] G. Baym, C. Pethick, and P. Sutherland, Astrophysical Journal 170, 299 (1971).
- [31] M. Brack, C. Guet, and H.-B. Håkansson, Phys. Rep. 123, 275 (1985).
- [32] M. M. Sharma, S. A. Moszkowski, and P. Ring, Phys. Rev. C 44, 2493 (1991).
- [33] D. Von-Eiff, J. M. Pearson, W. Stocker, and M. K. Weigel, Phys. Lett. B 324, 279 (1994).
- [34] D. Von-Eiff, W. Stocker, and M. K. Weigel, Phys. Rev. C 50, 1436 (1994).

- [35] D. Von-Eiff, H. Freyer, W. Stocker, and M. K. Weigel, *Phys. Lett. B* 344, 11 (1995).
- [36] M. Centelles, M. Del Estal, and X. Viñas, *Nucl. Phys. A* 635, 193 (1998).
- [37] M. Del Estal, M. Centelles, and X. Viñas, *Nucl. Phys. A* 650, 443 (1999).
- [38] S. K. Patra, M. Centelles, X. Viñas, and M. Del Estal, *Phys. Rev. C* 65, 044304 (2002).
- [39] P. Danielewicz and J. Lee, *Nucl. Phys. A* 818, 36 (2009).
- [40] M. B. Christiansen, N. K. Glendenning, and J. Schaffner-Bielich, *Phys. Rev. C* 62, 025804 (2000).
- [41] M. Alford, K. Rajagopal, S. Reddy, and F. Wilczek, *Phys. Rev. D* 64, 074017 (2001).
- [42] J. A. Rueda, R. Ruffini, Y.-B. Wu, and S.-S. Xue, *Phys. Rev. C* 89, 035804 (2014).
- [43] Y.-B. Wu, *J. Korean Phys. Soc.* 65, 850 (2014).
- [44] N. Bohr and J. A. Wheeler, *Phys. Rev.* 56, 426 (1939).
- [45] M. Rotondo, R. Ruffini, S.-S. Xue, and V. Popov, *Int. J. Mod. Phys. D* 20, 1995 (2011).
- [46] M. Rotondo, J. A. Rueda, R. Ruffini, and S.-S. Xue, *Phys. Rev. C* 83, 045805 (2011).
- [47] J. Boguta, *Phys. Lett. B* 106, 255 (1981).
- [48] M. Centelles, M. Pi, X. Viñas, F. Garcias, and M. Barranco, *Nucl. Phys. A* 510, 397 (1990).
- [49] H. Shen, H. Tokia, K. Oyamatsuc, and K. Sumiyoshi, *Nucl. Phys. A* 637, 435 (1998).
- [50] S. S. Avancini, L. Brito, J. R. Marinelli, D. P. Menezes, M. M. W. de Moraes, C. Providência, and A. M. Santos, *Phys. Rev. C* 79, 035804 (2009).
- [51] G. A. Lalazissis, J. König, and P. Ring, *Phys. Rev. C* 55, 540 (1997).
- [52] A. Tamii, *et al.*, *Phys. Rev. Lett.* 107, 062502 (2011).
- [53] P. Papakonstantinou, J. Margueron, F. Gulminelli, and Ad. R. Raduta, *Phys. Rev. C* 88, 045805 (2013).
- [54] F. Aymard, F. Gulminelli, and J. Margueron, *Phys. Rev. C* 89, 065807 (2014).
- [55] C. J. Horowitz and J. Piekarewicz, *Phys. Rev. Lett.* 86, 5647 (2001);
- [56] B.-A. Li, L.-W. Chen, and C. M. Ko, *Phys. Rep.* 464, 113 (2008).